The effect of blockage and tunnel slope on smoke spread and ceiling temperature distribution in a natural-ventilated metro depot

Jiaqiang Han[a,b], Zihao Wang[c], Pengqiang Geng[a], Fei Wang[a], Jennifer Wen[b], Fang Liu[a,d,e**]*

a School of Civil Engineering, Chongqing University, Chongqing, 400045, P.R. China;

b Warwick Fire, School of Engineering, University of Warwick, Coventry, CV4 7AL, UK;

c College of Environment and Ecology, Chongqing University, Chongqing, 400045, P.R. China;

d Key Laboratory of New Technology for Construction of Cities in Mountain Area of Ministry of Education (Chongqing University), Chongqing, 400045, P.R. China;

e Joint International Research Laboratory of Green Buildings & Built Environments, Chongqing, 400045, P.R. China;

**Corresponding author:*

Jennifer Wen: jennifer.wen@warwick.ac.uk, University of Warwick, Coventry, CV4 7AL, UK

Fang Liu: drliufang@126.com, Chongqing University, Shapingba District, 400045, P.R. China

Abstract

The current research investigated the coupling effect of blockage and tunnel slope on spreading characteristics of the fire smoke and ceiling temperature distribution in a metro depot with one closed end. A series of 1/15 reduced scale experiments and full-scale numerical simulations were conducted to capture the global fire characteristics. The investigation addressed and compared the effect of tunnel slopes on the fire plume behavior and ceiling temperature distribution in both uphill and downhill situations. The presence of the blockage upstream of the fire was further investigated to highlight the heat accumulation between the closed end and fire, and the associated effect on the pool fire mass burning rate. Comparison has been made between the ceiling temperature distribution of when the tunnel slope increases in both uphill and downhill tunnels. The coupling effect of blockage and tunnel slope was analyzed in relation to the maximum and extent of high temperature area on tunnel ceiling. Two empirical correlations have also been proposed to predict the maximum temperature and upstream temperature attenuation in a metro depot, accounting for the influence of blockage and tunnel slope. Comparison among the measurements, predicted values, literature models and data exhibit relatively good agreement.

***Keywords*:** Ceiling temperature; Blockage effect; Tunnel Slope; Closed portal; Metro fire

Nomenclature

Nomenclature	
$\dot{m}$	Burning rate (g/ s)
θ	Tunnel slope in percentage
Q	Heat release rate (kW)
V	Longitudinal ventilation velocity (m/s)
Q^*	Dimensionless heat release rate
V'	Dimensionless ventilation velocity
D^*	Character length of the fire (m)
D_r	Radius of fire source (m)
T_a	Ambient temperature (℃)
F_r	Froude number
S_t	Stanton number
H_t	Tunnel height (m)
W_t	Tunnel width (m)
A_t	Area of tunnel cross-section (m^2)
δx	Mesh size (m)
ρ_a	Air density (kg/m^3)
C_p	Specific heat of ambient air (kJ/kg·K)
H_{ef}	Effective tunnel height (m)
d_{fb}	Fire-block distance (m)
d_{fw}	Distance between fire and closed end (m)
ΔT	Temperature rise (℃)
ΔT_{max}	The maximum temperature (℃)
Subscript	
x_0	Reference point
x	Distance between the measuring point and reference point
f	Full-scale
m	Reduced scale
max, b	Maximum value considering blockage
max, fb	Maximum value considering fire-blockage distance
max, sb	Maximum value considering tunnel slope and blockage
Greek letters	
κ	Attenuation coefficient in Eq. (2)
ξ	Cross sectional coeffcient in Eq. (4)
γ	Coefficient in Eq. (5)
ε	Coefficient in Eq. (5)
μ_1	Width-block ratio in Eq. (9)
μ_2	Height-block ratio in Eq. (9)
ψ	Coefficient in Eq. (12)
λ_θ	Coefficient in Eq. (14)
k_θ	Coefficient in Eq. (14)

1. Introduction

In the last few decades, considerable metro lines were planned and constructed in China due to the growing demand for a safer and faster urban transportation. In the meantime, there is also a growing need releasing the pressure on the land traffic. This has motivated plenty of underground tunnels being constructed to build up a comprehensive traffic network. Inside tunnels, no matter the fossil-consumer or the fuel-cell vehicles are running (Seike et al., 2019), fire safety is always the uppermost concern throughout the whole lifetime of a tunnel (Cheng et al., 2020). Usually, fires are deemed as unsteady and uncontrollable energy releases, (Nævestad and Meyer, 2014) which result in massive injuries, huge property losses, and considerable damage to the tunnel structure. Besides, fires are also very sensitive to the environmental conditions, e.g., wind and heat feedback. Fire prevention and smoke control within underground tunnels is thus very difficult as the ventilation and traffic condition often leads to a more complex flow filed compared to that in the other buildings (An et al., 2021). To effectively control the smoke spread and reduce the risk of large-scale casualties and damages in fire situations, a comprehensive understanding about tunnel fire dynamics in natural ventilation situation is vital for the further designs of tunnel ventilation system (Barbato et al., 2014).

Previously, considerable investigations have been conducted to address the fire and smoke dynamics in tunnels, covering many different aspects including the burning characteristics (Ingason and Li, 2019), fire flame behavior (Shi et al., 2020), and smoke prevention (Yu et al., 2020). Ceiling temperature profiles, in particular, have been extensively investigated as it is one of the most representative indexes which can be linked to the tunnel structure damage, as well as the core factor to characterize the fire and smoke spread. Needless to say that the techniques for temperature measurements are relatively mature and can be radially implemented. Delichatsios (1981) theoretically identified three different regions to describe the smoke flowing characteristic under a beamed ceiling and proposed the following correlation to predict the fire induced ceiling temperature in a corridor-like enclosure:

$$\frac{\Delta T_x}{\Delta T_{x_0}}\left(\frac{W_t}{2H_{ef}}\right)^{1/3} = 0.49exp\left[-6.67S_t\frac{x}{H_{ef}}\left(\frac{W_t}{2H_{ef}}\right)^{1/3}\right] \quad (1)$$

where ΔT is temperature rise, x_0 denotes the reference point and x represents the distance between the measuring point and reference point, W_t is the tunnel width, H_{ef} is the effective tunnel height, and S_t is Stanton number with value of 0.03. By conducting theoretical analysis and

full-scale burning tests, Hu et al. (2005) established the following simple formula to predict temperature decay of a tunnel fire:

$$\frac{\Delta T_x}{\Delta T_{x_0}} = exp^{-\kappa x} \tag{2}$$

where κ is the attenuation coefficient determined by the experimental data. Through reduced scale tests with various heat release rates and ventilation velocities, Ingason and Li (2010) demonstrated that ceiling temperature in tunnels with low ventilation velocity could be generated as:

$$\frac{\Delta T_x}{\Delta T_{x_0}} = 0.57exp^{-0.13\frac{x}{H_t}} + 0.43exp^{-0.021\frac{x}{H_t}} \tag{3}$$

where H_t is tunnel height. Thereafter, by introducing the cross sectional coefficient ξ, Liu et al. (2016) considered nine typical tunnel cross-sections based on the survey of metro line 6 in Chongqing, China and proposed the following expressions to quantify the influence of tunnel cross-section on the ceiling temperature profiles:

$$\begin{cases} \frac{\Delta T_x}{\Delta T_{x_0}} = exp^{-(0.343\,\xi)\frac{x}{H_t}} & ,\xi \geq 1.0 \\ \frac{\Delta T_x}{\Delta T_{x_0}} = exp^{-(0.104\xi - 0.215)\frac{x}{H_t}} & ,\xi < 1.0 \end{cases} \tag{4}$$

where $\xi = \frac{A_t}{H_t^2}$.

More recently, Tang et al. (2020) investigated the lateral ceiling temperature profiles in a 1/8 scaled model tunnel considering wall fires with different aspect ratios. Formulas predicting the flame extension length and temperature distribution were put forward. Some scholars also addressed other influencing factors like the wall properties (Saito and Yamauchi, 2021) and fire location (Fan et al., 2015).

In the event of a fire in tilted tunnels, smoke spread and ceiling temperature distribution behave differently due to the stack effect. Atkinson and Wu (1996) claimed that a stronger longitudinal ventilation velocity should be produced to suppress the upwind smoke propagation in a downhill tunnel with tunnel slope varying from 0° to 10°. Based on the empirical models proposed by Kurioka et al. (2003) and Li et al. (2011), Hu et al. (2013) established two modified formulas, generated as Eq. (5), to calculate the maximum temperature in a titled tunnel. Meanwhile, a further formula to generate the temperature decay was also proposed as Eq. (6).

$$\frac{\Delta T_{max}}{T_a} = (1 - 0.077\theta) \cdot \gamma \left(\frac{{Q^*}^{2/3}}{{F_r}^{1/3}}\right)^{\varepsilon} \tag{5-a}$$

$$\Delta T_{max} = \begin{cases} (1 - 0.067\theta) \frac{Q}{V {D_r}^{1/3} H_{ef}^{5/3}}, & V' > 0.19 \\ (1 - 0.061\theta) \cdot 17.5 \frac{Q^{2/3}}{H_{ef}^{5/3}}, & V' \leq 0.19 \end{cases} \tag{5-b}$$

$$\frac{\Delta T_x}{\Delta T_{max}} = exp^{-(1+0.09\theta)\cdot\kappa x} \tag{6}$$

where ΔT_{max} denotes the maximum temperature, T_a is the ambient temperature, θ is tunnel slope in percentage, γ and ε are coefficients, Q is heat release rate, Q^* is dimensionless heat release rate, F_r represents Froude number, V is longitudinal ventilation velocity, D_r is radius of fire source, and V' denotes dimensionless ventilation velocity, respectively. The above correlations imply that both the maximum temperature and ceiling temperature decreases with the increase of tunnel slope θ. Through dimension analysis and FDS numerical simulation, Wang et al. (2020) further explored the influence of tunnel width on the temperature distribution. Measurements from simulations yielded that the downstream temperature attenuation could be well estimated by:

$$\frac{\Delta T_x}{\Delta T_{x_0}} = 0.46exp^{-(0.95+4.69\theta)\frac{xW_t}{H_t^2}} + 0.54exp^{-(0.038+0.17\theta)\frac{xW_t}{H_t^2}} \tag{7}$$

Most of the aforementioned studies, i.e., Delichatsios (1981), Hu et al. (2005), Ingason and Li (2010), Hu et al. (2013), Liu et al. (2016), and Wang et al. (2020), addressed fire scenarios in tunnels without any obstacles inside. However, the blockage effect is a very practical issue in metro tunnel fires due to the passing or parking of the metro trains (Rojas Alva et al., 2017; Shafee and Yozgatligil, 2018a). In such situation, heat feedback from the tunnel structure, surroundings and ventilation effect are all influenced by the presence of running or stationary metro trains. Early research on the blockage effect could be traced back to the end of the last century and was predominately related to longitudinal ventilation. Oka and Atkinson (1995) firstly investigated the blockage effect in a longitudinally ventilated tunnel and demonstrated that the critical velocity dropped by 15% when the blockage occupied 12% of tunnel cross-section and by 40%~45% if the vehicles occupied 32% of the tunnel cross-section. Through reduced scale experiments, Li et al. (2010) obtained similar conclusion with Oka and Atkinson (1995) and established simple expressions to calculate the critical velocity. Tang et al. (2017) studied the maximum temperature regarding the fire-blockage distance in a longitudinal ventilated tunnel and proposed an empirical formula to calculate the maximum temperature as:

$$\Delta T_{max,fb}=\begin{cases}\frac{Q}{\lambda v r^{1/3}H_{ef}^{5/3}}\left(0.42d_{fb}+1.15\right) & V'>0.19,\ d_{fb}\le 0.5\\ \frac{Q}{\lambda v r^{1/3}H_{ef}^{5/3}}\left(-0.23d_{fb}+1.48\right) & V'>0.19,\ 0.5<d_{fb}\le 2.5\\ \frac{Q}{v r^{1/3}H_{ef}^{5/3}} & V'>0.19,\ d_{fb}>2.5\\ \left(0.41d_{fb}+1.08\right)\cdot 17.5\frac{Q^{2/3}}{H_{ef}^{5/3}} & V'\le 0.19,\ d_{fb}\le 0.5\\ 17.5\frac{Q^{2/3}}{H_{ef}^{5/3}} & V'\le 0.19,\ d_{fb}>0.5\end{cases} \quad (8)$$

where $\Delta T_{max,fb}$ represents the maximum temperature considering fire-blockage distance d_{fb}. More recently, Wang et al. (2021) numerically studied the effect of heat release rate, blockage length, and block ratios, i.e., width-block ratio μ_1 and height-block ratio μ_2 on smoke movement and ceiling temperature. Measurements yielded that the maximum temperature in the presence of blockage could be well correlated by:

$$\Delta T_{max,b}=16.9(-0.487\mu_1+0.573\mu_2+1.239)\cdot\left(1+0.299exp^{-0.793\frac{d_{fw}}{H_{ef}}}\right)\cdot\frac{Q^{2/3}}{H_{ef}^{5/3}} \quad (9)$$

where $\Delta T_{max,b}$ is the maximum temperature considering block ratio and d_{fw} denotes the longitudinal distance between the fire and closed end. Besides, some investigations have also been reported about the effect of blockage on smoke behavior (Waman and Harish, 2020), thermal stratification (Gannouni et al., 2019), and critical velocity (Gannouni and Maad, 2015).

Despite the above progress, the effect of blockage on fire spread and smoke movement in titled tunnels have been largely overlooked. The present study is motivated by the need to fill this knowledge gap. Seventeen reduced scale experiments and forty full-scale CFD simulations were conducted in a natural-ventilated metro depot designed with one closed end, the experimental and numerical investigation of which have been reported in our previous studies (Han et al., 2021; Wang et al., 2021). To be noted, fire safety problems in the metro depot with one closed end has indeed attracted considerable attention in recent years. Similar concern has also been given to the structures like subway station (Ji et al., 2011), utility tunnel (Gao et al., 2021), tunnel under construction (Mehaddi et al., 2020), and corridor-like enclosure (Ishikawa et al., 2020). Fires in such type of underground buildings can potentially result in much more severe heat accumulation near the closed end as smoke emission is greatly restrained.

The novelties of this work are: 1) revealing the blockage effect on flame behavior and burning rate of pool fires burned in natural-ventilated tunnels with one closed end; 2) investigating the

coupling effect of blockage and tunnel inclination on the ceiling temperature. Correspondingly, outcomes of the present study are expected to 1) deepen the understanding of pool fire burning characteristics accounting for the blockage effect and tunnel slope and to help engineers estimate the fire development precisely; 2) offer a theoretical reference to better capture the spread of ceiling temperature and to aid the design of tunnel ventilation system in such tunnels and other underground spaces.

2. Experiments

2.1 Scaling law

Reduced scale experiments are often used to simulate the real fire scenarios due to its lower cost compared to the full-scale experiments. Measurements can be meaningful if the model test bed is designed with appropriate scaling laws. The basic conditions dominating the conversion from model-test measurements to full-scale include geometric similarity, kinematic similarity, and dynamic similarity. However, it is usually impossible to simultaneously obtain these three similarities. Froude number, the ratio of inertial force and buoyancy force, is often utilized to achieve the dynamic similarity in fire or smoke tests (Ingason et al., 2015). By holding Froude number as a constant value, conversion of the key parameters utilized in the current study are listed as:

$$\frac{Q_m}{Q_f} = \left(\frac{L_m}{L_f}\right)^{5/2} \tag{10-a}$$

$$T_m = T_f \tag{10-b}$$

$$\frac{V_m}{V_f} = \left(\frac{L_m}{L_f}\right)^{1/2} \tag{10-c}$$

$$\frac{t_m}{t_f} = \left(\frac{L_m}{L_f}\right)^{1/2} \tag{10-d}$$

where Q represents heat release rate, L, T, V and t respectively denote length, temperature, velocity, and time. In the past few decades, the credibility of using Froude similarity laws has been extensively validated by considerable investigations (Ingason and Li, 2010; Tanaka et al., 2015).

2.2 Experimental scheme

Figure 1 displays a sketch view of the 1/15 scaled model test bed. It was consisted of five

individual units with dimension of 1.0 m (length) × 0.32 m (width) × 0.48 m (height). Tinfoil was utilized to bound the joints of each two units to ensure the airtightness. The test bed was constructed with a closed portal referring to the metro depot reported in our previous research (Han et al., 2020; Wang et al., 2021). To be clarified, the 5.0 m long model tunnel utilized in the present work is deemed as effective to conduct the investigation in the regard of pool fire burning behavior and temperature spreading characteristics according to the research of Ishikawa et al. (2020). Three materials, namely steel board (tunnel ceiling and floor), calcium silicate board (closed portal) and fireproof glass (sidewalls) composed its supporting structure.

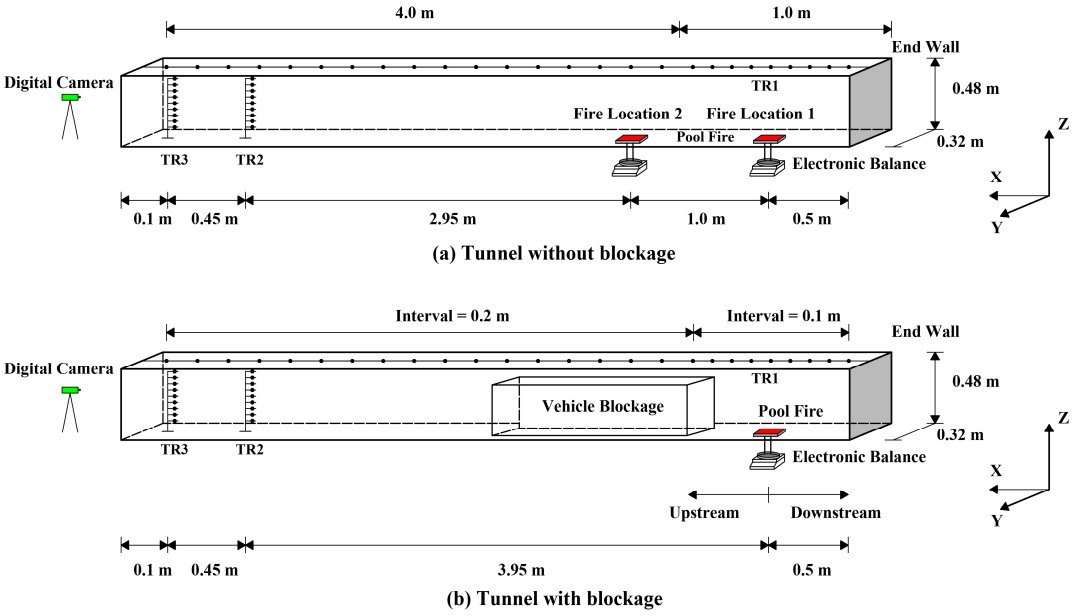

Figure 1. Schematic view of test bed and apparatus.

Inside the model tunnel, the vehicle blockage built with steel plates having a dimension of 0.60 m×0.20 m×0.25 m or 0.60 m×0.15 m×0.30 m was placed 0.2 m upstream the fire to simulate the blockage effect. Three strings of K-type thermocouples of 5 mm thickness, namely TR1, TR2, and TR3, were installed inside the model tunnel for temperature measurements. To simplify the description of the location of measuring devices, X, Y, and Z respectively represents the axis at longitudinal, transverse, and vertical direction (as shown in Figure 1) without specification. Two sets of thermocouples numbered from THCP01 to THCP29 in TR1 were placed 0.02 m underneath the ceiling along the longitudinal centerline. Probes THCP01 - THCP09 in the first set of TR1 distributed within X=0.1 m to X= 0.9 m at the interval of 0.1 m while the rest probes THCP10 - THCP29 located within X=1.1 m to X= 4.9 m at the interval of 0.2 m. TR2 (probes THCP30 -

THCP38) and TR3 (probes THCP39 - THCP47) were thermocouple trees located at X=4.45 m and X=4.90 m, respectively. Each thermocouple tree held nine probes installed from Z=0.05 m to Z=0.45 m at the interval of 0.05 m. Temperatures in every test were documented by a data logging system and values were output every 10 s. Moreover, each burning test was repeated twice and the averaged values generated from the quasi-steady state (see in Figure 2) were obtained for further analysis and calculation. A digital camera with the assistance of the laser sheet was used to record the fire evolution and smoke propagation. Additionally, uncertainty analysis of the measurements is given in the Appendix.

As for the fire system, five pool sizes, i.e., 8 cm×8 cm, 10 cm×10 cm, 12 cm×12 cm, 15 cm×15 cm, and 15 cm×20 cm, were designed to generate multiple heat release rates. For the rectangular fuel pans, the long side was parallel to the Y axis. The duration of the fire was controlled by the initial quantity of ethanol for each fuel pan as 75 ml, 125 ml, 175 ml, 250 ml, and 300 ml (with less than $\pm$ 5 ml in error). In each test, fuel burning rate of the pool fire was recorded by an electronic balance with accuracy of 0.01 g. Readings were timely transferred to a laptop computer every 2 s. The heat release rate was obtained by multiplying the specific heat of combustion by the average value of burning rate at quasi-steady state. The calculated heat release rates correspond to the full-scale equivalent size are within 2.0 MW~13.0 MW. Figure 2 illustrates how the quasi-steady state was determined and how the burning rate and temperature data (THCP05) were averaged. Clearly, measurements denote very small fluctuation between 350 s to 550 s in Figure 2-(a) and between 300 s to 600 s in Figure 2-(b). Measurements within these two periods were hence used to derive the average values for corresponding data. It should be noted that measurements of burning rate and temperature in Figure 2-(a) are higher than that in Figure 2-(b). This is thought to be due to the enhanced heat feedback caused by the blockage effect and will be discussed in more details in the later section.

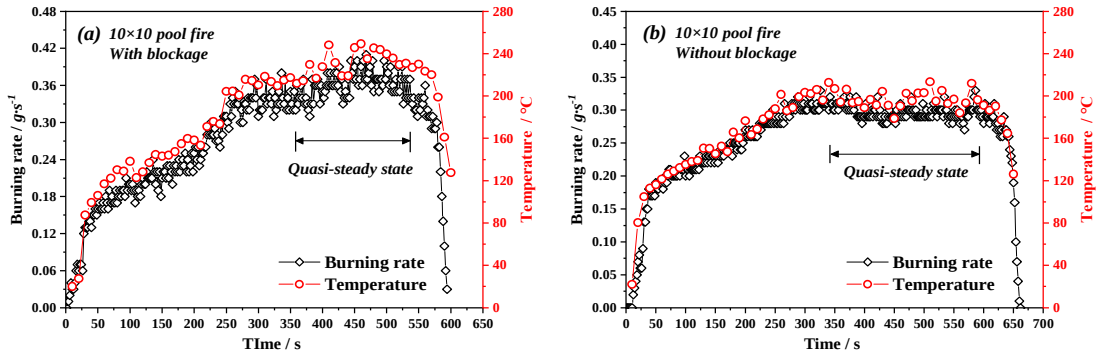

Figure 2. Averaged values obtained from quasi-steady state.

Table 1. Experimental scheme.

Test No.	Pool Size (cm×cm)	Blockage (m×m×m)	d_{fb} (m)	d_{fw} (m)	Ventilation Mode
A01-A10	8×8, 10×10, 12×12 15×15, 15×20	/	/	0.5, 1.5	Natural Ventilation
A11-A15	8×8, 10×10, 12×12 15×15, 15×20	0.60×0.20×0.25	0.2	0.5	Natural
A16-A17	12×12, 15×15	0.60×0.15×0.30	0.2	0.5	Ventilation

As shown in Table 1, a total number of seventeen reduced scale tests were conducted in two sets. Pool fires in the first set were located at different d_{fw} to the closed end and burned without the blockage. In the second set, two cuboid vehicle models were constructed and placed 0.2 m upstream of the fire to simulate the blockage effect. The model tests only covered the pool fires burned in a flat model tunnel while the titled tunnel was investigated by CFD simulations only.

3. Numerical set-up

3.1 Introduction of FDS

The NIST Fire Dynamic Simulator, simply known as FDS (McGrattan et al., 2018), was used for the current study. The code has been widely utilized by the fire community, e.g., Liu et al. (2019), Liu et al. (2020). FDS is based on the Large Eddy Simulation (LES) approach. In the present simulations, the Deardorff's model (McGrattan et al., 2018), which is the default sub-grid scale (SGS) turbulence model, was employed to deal with the turbulence issue. The default radiation

model was used. As for the combustion, reaction between the ethanol and oxygen was assumed to be infinitely fast. The simple chemistry, mixing-controlled chemical reaction (single-step) which uses three lumped species was adopted to deal with the combustion reaction, i.e., $C_2H_5OH + v_{O_2}O_2 + v_{N_2}N_2 \rightarrow v_{CO_2}CO_2 + v_{H_2O}H_2O + v_{CO}CO + v_sSoot + v_{N_2}N_2$. The soot and CO yields were specified as zero as the combustion of ethanol was assumed to be fully developed (Zukoski et al., 1981; Ji et al., 2012).

3.2 Model Set-up and Boundary Conditions

As shown in Table 2, two sets (simply known as B and C set) of numerical simulations were conducted. The B set simulations were carried out at reduced scale for model validation with experimental measurements using the same physical dimensions and boundary conditions as experimental conditions described in Section 2. In addition, heat release rates in B set simulations were defined by mass loss rate instead of heat release rates per unit area (HRRPUA). Values of mass loss rate used for each simulation were kept same as experimental measurements (summarized in Table 3).

The C set modelled the full-scale tunnel of 200 m long, 4.8 m wide and 7.2 m in height. As shown in Figure 3, an extended cubic domain with diameter of 10.0 m was additionally attached to the tunnel opening portal to improve the boundary solution (Wang et al., 2006). Concrete was utilized as the wall material with density, specific heat, and conductivity respectively being 2200.0 kg/m^3, 1.04 kJ/kg·k, 1.8 W/m·k. Inside the tunnel, a single metro train carriage was placed 5.0 m upstream of the fire with dimension of 20.0 m×2.8 m×5.0 m, referring to the typical AS type metro train utilized in Chongqing Rail Transit. Steel was used as the material of the metro carriage with density, specific heat, and conductivity being 7850.0 kg/m^3, 0.46 kJ/kg·k, 45.8 W/m·k. A full-length metro marshalling was not used here because previous studies (Zhang et al., 2020; Wang et al., 2021) suggested that the train length had very limited influence on both smoke movement and ceiling temperature distribution. In addition, intervals of tunnel slope in Test C06-C19 and Test C27-C40 are set as 1%.

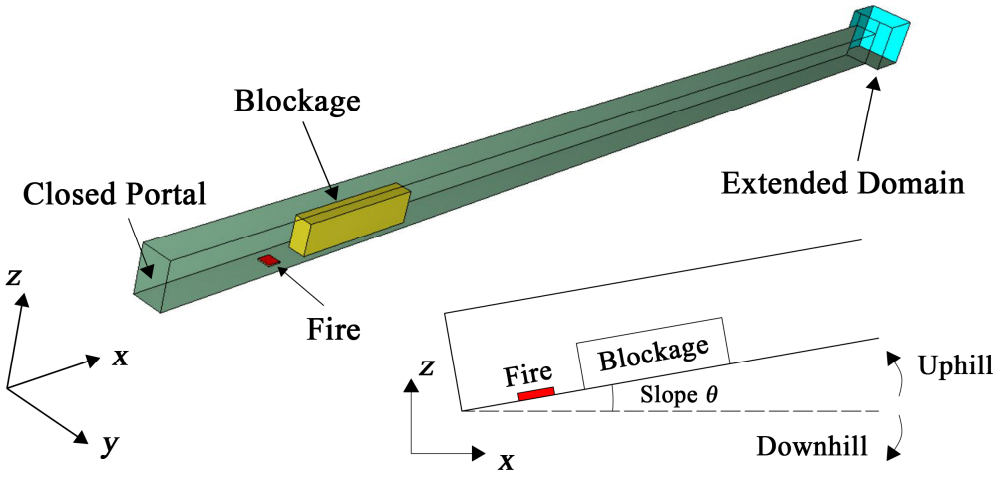

Figure 3. 3D and slice views of the full-scale model in simulation.

Table 2. Simulation scheme.

Test No.	Slope (%)	HRR (MW)	Blockage (m×m×m)	d_{fw} (m)	Ventilation Mode
B01 - B05	0	Same as	Without blockage	0.5	Natural
B06 - B10	0	experiments	0.60×0.20×0.25	0.5	ventilation
C01 - C05	0	1, 2, 4, 6, 8	Without blockage	20	
C06 - C12	0 - 6	1			
C13 - C19	0 - 6	2			Natural
C20 - C26	-6, -4 -2, 0, 2, 4, 6	4	20.0×2.8×5.0	20	ventilation
C27 - C33	0 - 6	6			
C34 - C40	0 - 6	8			

Fires were placed 20.0 m to the closed end with five heat release rates produced by the square burners which were prescribed with different heat release rates per unit area (HRRPUA). Corresponding to the burner diameters being 1.0 m for 1.0 MW and 2.0 MW fires and 2.0 m for the rest, the prescribed values were 1000, 2000, 1000, 1500, and 2000 kW/m^2, respectively. The lower and upper limit of the fire load utilized in the present research are respectively 1.0 MW and 8.0 MW. The lower limit, i.e., 1.0 MW, was designed to simulate the luggage fire which is very common to see in the subway system. Usually, the maximum fire size of a luggage fire is deemed to be less than 3.0 MW (Long et al., 2020). The 1.0 MW fire adopted here was to provide a more comprehensive illustration of subway fire scenarios by using a wider range of fire sizes. The maximum fire load in

simulations is 8.0 MW, exceeding the maximal heat release rate of a metro train fire reported as 5.0 MW by Liu et al. (2016).

Tunnel slope in the current work was achieved by separately defining the gravity component along each axis, e.g., for the tunnel slope equivalent to 2%, the gravity components were -9.808 along Z axis and -0.1962 along X axis. Without specification, the negative component along X axis represented the uphill tunnel and the positive one denoted the downhill tunnel. A clear illustration to identify the uphill and downhill tunnels can be seen in Figure 3. The overall simulation time was 150 s and the ambient temperature was 20 ℃. A summary of the simulation scheme is given in Table 2.

3.3 Computational grid and validation

Adequate computational grid is essential to achieve the compromise between accuracy and simulation time. McGrattan et al. (1998) suggested the dimensionless quantity D^*/δ_x as an influential factor to determine how well the flow field is solved when simulating a buoyant plume related problem.

$$D^* = \left(\frac{Q}{\rho_a C_p T_a g^{1/2}}\right)^{2/5} \tag{11}$$

where D^* is the character length of the fire, δx is the mesh size, ρ_a is the ambient air density, C_p is heat capacity of air, respectively. The range of D^*/δ_x was recommended as 4∼16 by McGrattan et al. (1998). Correspondingly, the proper diameter of the cubic mesh grid in this paper distributes within 0.07-0.38 m. The grid size equals to 0.10 D^*, in particular, was found to improve the prediction in comparison with the measurements. To maintain the accuracy while saving the simulation time, for the fire with heat release rate over 2.0 MW δx was set as 0.20 m, respectively denoting $0.11D^*$ (4.0 MW fire), $0.09D^*$ (6.0 MW fire), and $0.08D^*$(8.0 MW fire). As for the 1.0 MW and 2.0 MW fires, δx within the fire region (from X=10.0 m to X=25.0 m) was set as 0.10 m, representing $0.09D^*$ (1.0 MW fire) and $0.07D^*$ (2.0 MW fire). For the rest of computational domain, half the fine grid resolution, i.e., δ_x=0.20 m, was utilized. The credibility of using such hybrid meshes has been validated by previous scholars, e.g., Huang et al. (2018) and Liu et al. (2020). In Figure 4, the simulated and measured ceiling temperature distributions are compared and show relatively good agreement.

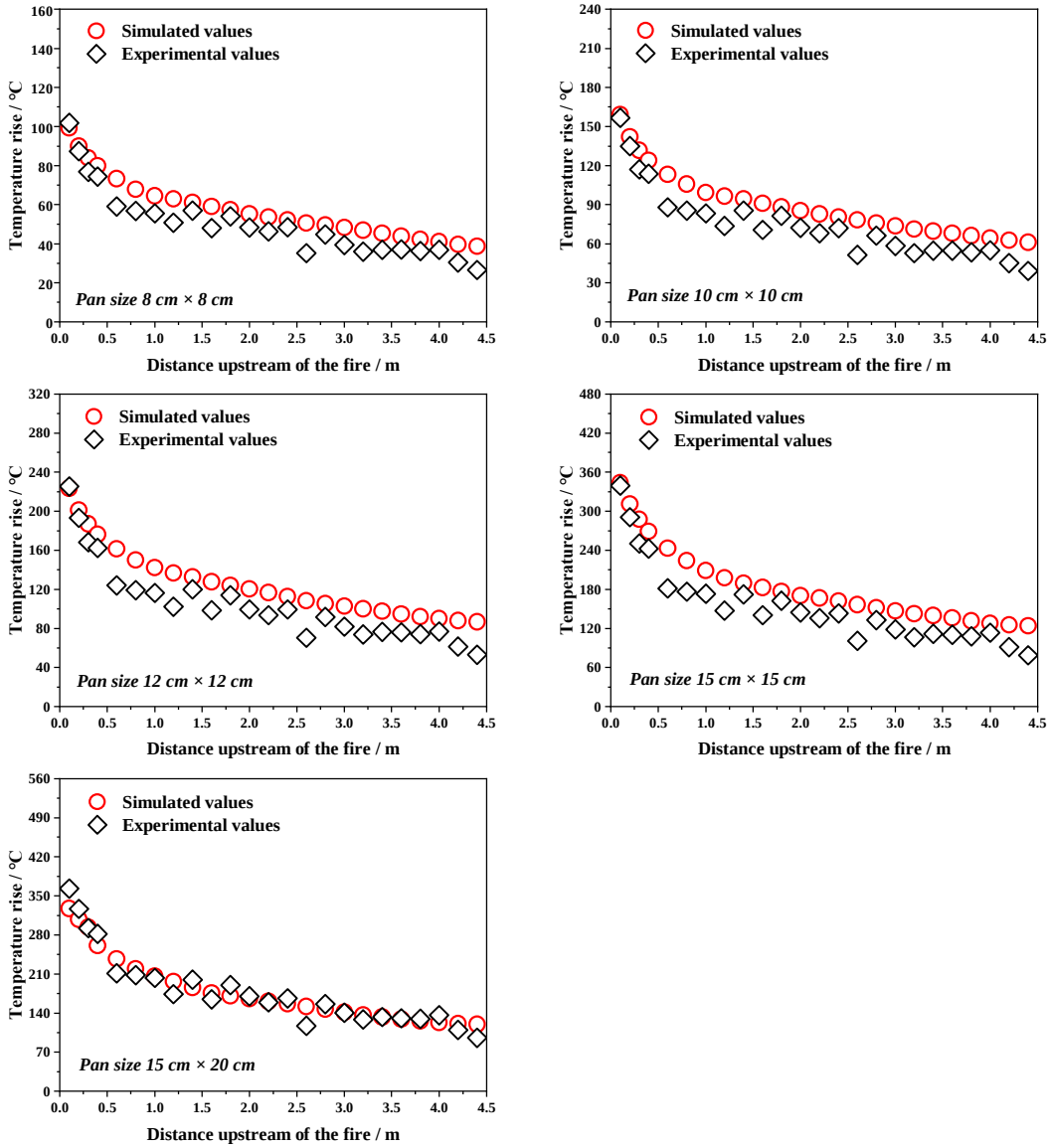

Figure 4. The simulated and measured ceiling temperature distributions.

4. Results and discussion

4.1 Effects of blockage

Blockage was found to influence the pool fire burning behavior (Shafee and Yozgatligil, 2018a) and thermal characteristics (Tang et al., 2017) as heat feedback and ventilation effect change in the presence of blockage near the fire source. In this section, flame shape, burning rate, and ceiling temperatures are discussed in turn to clarify the influence of blockage effect.

Figure 5 exhibits the instantaneous flame shapes of the pool fires burned with and without

blockage. The fire flame tends to lean towards the closed end in Figure 5-(a) where the pool fire burns without blockage. This is due to the asymmetric flow characteristics caused by the closed end (Han et al., 2020) and fire location (Yao et al., 2017). When the fire burns near the closed end, smoke gathering between the fire and closed end becomes more severe, resulting in a higher temperature and lower gas density. On the contrary, smoke emission through the opening portal unloads massive heat, leading to lower temperature and higher gas density between the fire and tunnel portal. Such gas density difference on the two sides of the fire causes the asymmetric pressure condition which finally drives the fire plume inclining towards the closed end. However, when the blockage is placed 0.2 m upstream of the fire, flame shown in Figure 5-(b) begins swinging and fails to maintain the stable inclination. This is likely because the asymmetric pressure condition on the two sides of the fire has been disturbed by the blockage. Balance of the heat feedback on the two sides of the fire is hard to achieve as it depends on many factors, e.g., fire-closed end distance d_{fw}, fire-blockage distance d_{fb}, materials of the closed end and blockage, etc. Besides, the ventilation effect at the vicinity of the fire is another reason to cause the swing of the flame. Without blockage, a clear stratification drives smoke flowing along the upper part of the tunnel while the induced airflow occupying the lower part. In the presence of the blockage, velocity of the induced airflow near the blockage increases due to the narrowing of the cross-section area. Correspondingly, this aggravates the turbulence near the fire, rendering it more unstable.

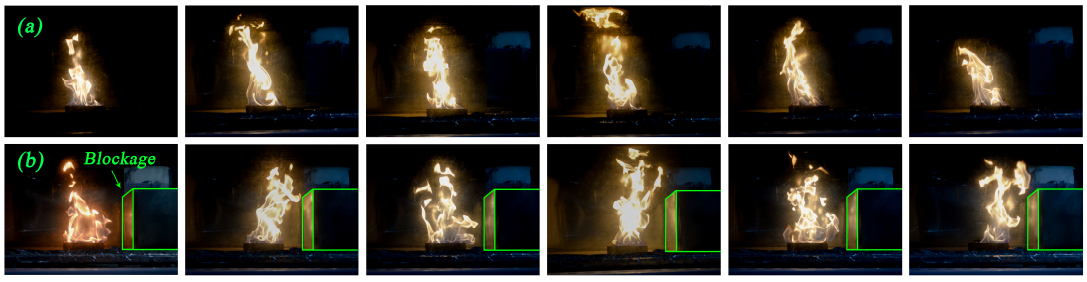

Figure 5. Flame shape affected by the blockage effect:
a) without blockage (A05); b) with blockage A (A15).

To further explore the influence of the blockage on the thermal properties of the fire plume, temperature contours of B05 and B10 in B set simulations, which correspond to the reduced scale tests A05 and A15, are plotted in Figure 6. Results indicate distinct differences in terms of the fire plume behavior, smoke movement, and thermal stratification characteristics. In line with the

observations in the model tests shown in Figure 5, the fire plumes in Figure 6 tends to lean towards the closed portal without blockage and temporarily inclined towards the blockage placed 0.2 m upstream of the fire. Meanwhile, the simulated temperature contours indicate difference in the pattern of ceiling smoke impingement due to the blockage effect. If simply defining the temperature region within 350 ℃~400 ℃ as the smoke plume region, it is reasonable to conclude that the total length of the smoke plume impingement increases as blockage occurs. In other words, the blockage results in the increase of high temperature area, e.g., the maximum temperature of Figure 6-(a) is within 350 ℃~400 ℃ while it exceeds 400 ℃ when the blockage presents in Figure 6-(b). The reason behind is due to the increase of fuel burning rate, i.e., the increase of heat release rate leads to higher ceiling temperatures. Essentially, the increase of fuel burning rate can be explained by the following reasons. Firstly, the direct entrainment between inlet airflow and fire plume is hindered by the blockage, leading to the weakening of the cooling effect and unfavorable smoke emission. Correspondingly, heat accumulation within the fire region (between the closed end and blockage) is then significantly enhanced. Pool surface thus received much more heat feedback from the surroundings and then fuel burning rate increases due to the acceleration of fuel evaporation. Furthermore, the interface of the smoke-air layer is slightly elevated in the presence of the blockage, implying enhanced thermal stratification upstream of the fire due to the blockage effect. This perhaps because the plume entrainment near the fire is weakened due to the occurrence of blockage, which leads to the decrease of smoke quantity and thinner smoke layer thickness.

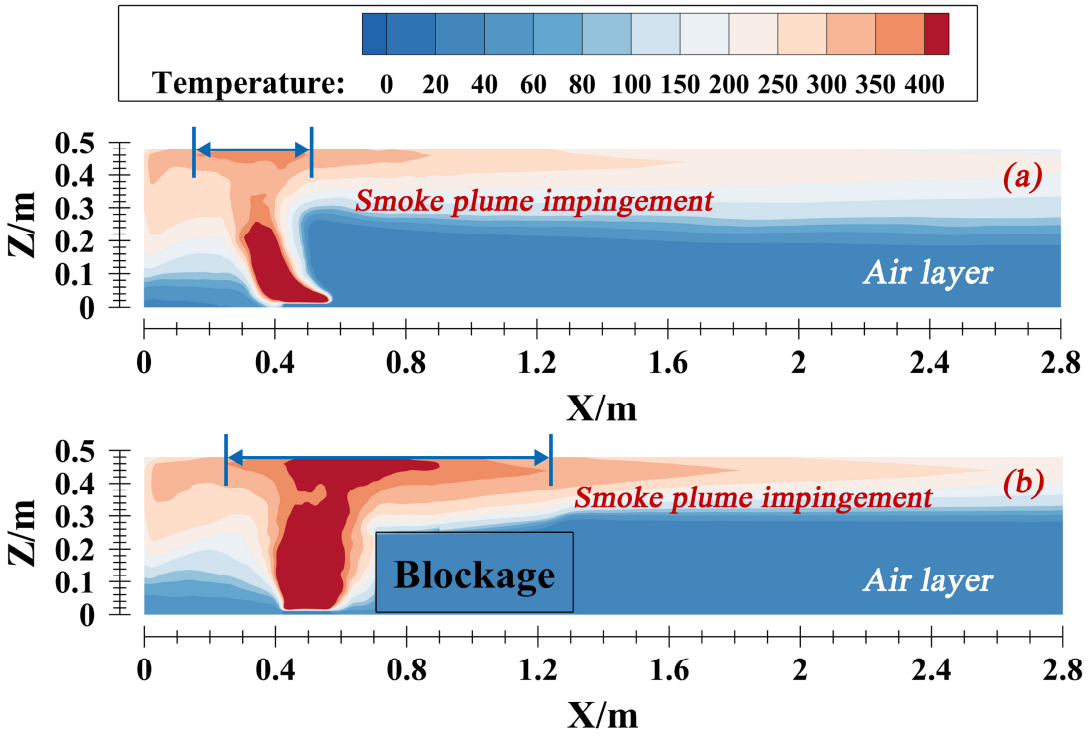

Figure 6. Zoom-in view of temperature contours: effect of blockage (B05 and B10).

The history of burning rate measured in experiments is exhibited in Figure 7 where results denote a generally similar burning tendency but a slight increase of burning rate and the decrease of burning duration caused by the blockage effect. The increase of burning rate is mainly caused by the increase of heat feedback which pool fires obtained from the surface of blockage. Meanwhile, temperature between the fire and blockage rises up as the cooling effect is enfeebled, due to which fuel evaporation is accelerated and the burning period is shortened.

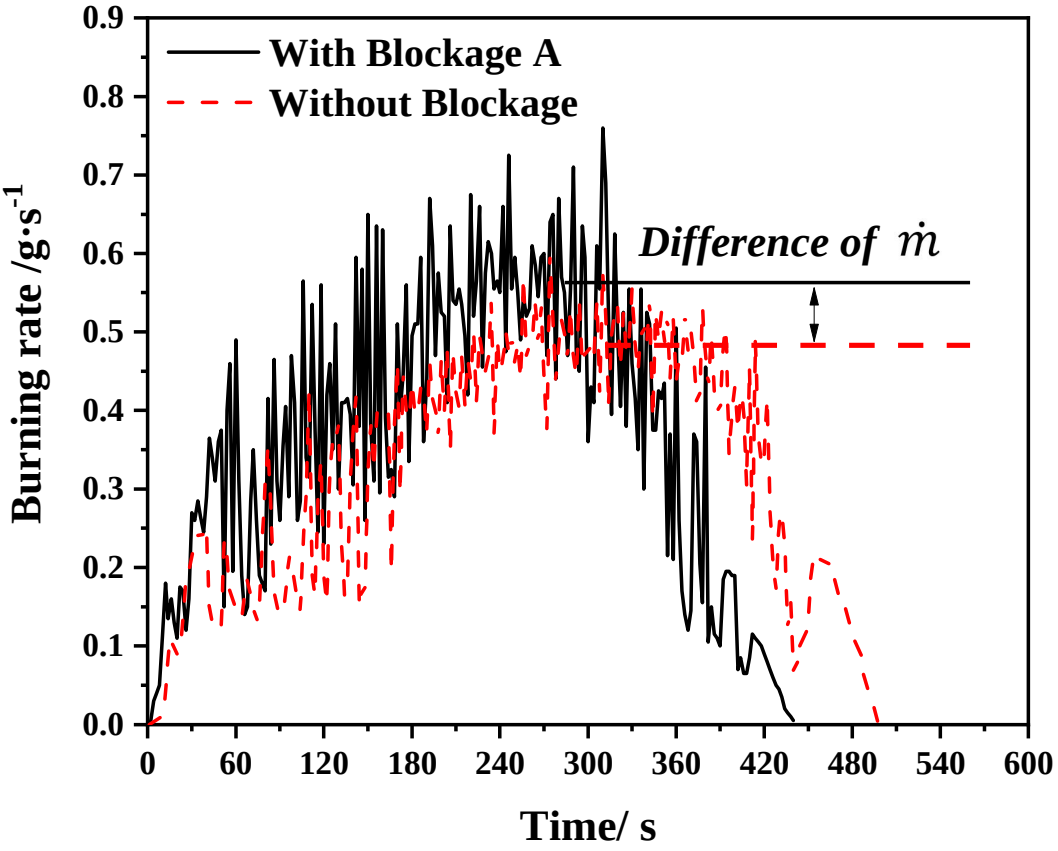

Figure 7. Burning rate affected by the blockage effect (pool fire 15 cm × 20 cm for instance).

Table 3. Burning rates $\dot{m}$ in the reduced scale experiments.

Pan Size (cm × cm)		Without Blockage		Blockage A	Blockage B
Length	Width	(A01-A05)	(A06-A10)	(A11-A15)	(A16-A17)
8	8	0.082	0.086	0.166	/
10	10	0.147	0.155	0.183	/
12	12	0.234	0.246	0.270	0.248
15	15	0.395	0.394	0.439	0.406
20	15	0.491	0.514	0.555	/

Table 3 summarizes burning rates measured in reduced scale tests. When the fire location change from d_{fw} =0.5 m to d_{fw} =1.5 m, variation of burning rate is insignificant. This is probably because pool fires in these two set experiments obtained generally equal heat feedback from the rim walls. Even though fuel burning rate may be affected by the closed portal, the previous report from Gao et al. (2014) indicated that such influence is still indistinct if the fire-wall distance is over 0.5 m. Nevertheless, with Blockage A placed 0.2 m upstream of the fire, burning rates increase between

0.03~0.04 g attributed to the enhanced heat feedback from the blockage surface. Furthermore, it is very interesting to find out that the average increase of burning rate caused by Blockage B is only about 0.01 g, which is relatively small compared to the values resulted by Blockage A. This is probably because Blockage A has a larger cross-section area than Blockage B, providing larger heat feedback to the fire to accelerate the fuel evaporation.

From the above analysis, it is reasonable to deduce that blockage certainly has impacts on the ceiling temperature profiles because the dominated factor, i.e., burning rate, increases as blockage occurs. Since the closed end and blockage effect are rarely simultaneously investigated in the previous researches, the published predictions and experimental measurements from similar fire scenarios, including the typical tunnel fire (Li et al., 2011), underground space with one closed end (Ji et al., 2011; Gao et al., 2021), tunnel with two closed ends (Yao et al., 2017), and tunnel with blockage (Tang et al., 2017; Wang et al., 2021), are plotted together with the present measurements in Figure 8. In general, the plotted values show similar trends. The present measurements, in particular, are found to agree very well with the predictions proposed by Wang et al. (2021) but slightly higher than the other models or data. This is mainly because the fire scenarios investigated in Wang et al. (2021)'s research, i.e., fire burns between the closed end and blockage, are highly coincide with the fire scenarios explored herein while heat accumulation caused by these two factors are not addressed in the other plotted data. Hence, in the following investigation, Eq. (9) which was correlated by Wang et al. (2021) from their measurements is directly used to calculate the maximum temperature in the horizontal tunnels with the fire burned between the closed portal and blockage.

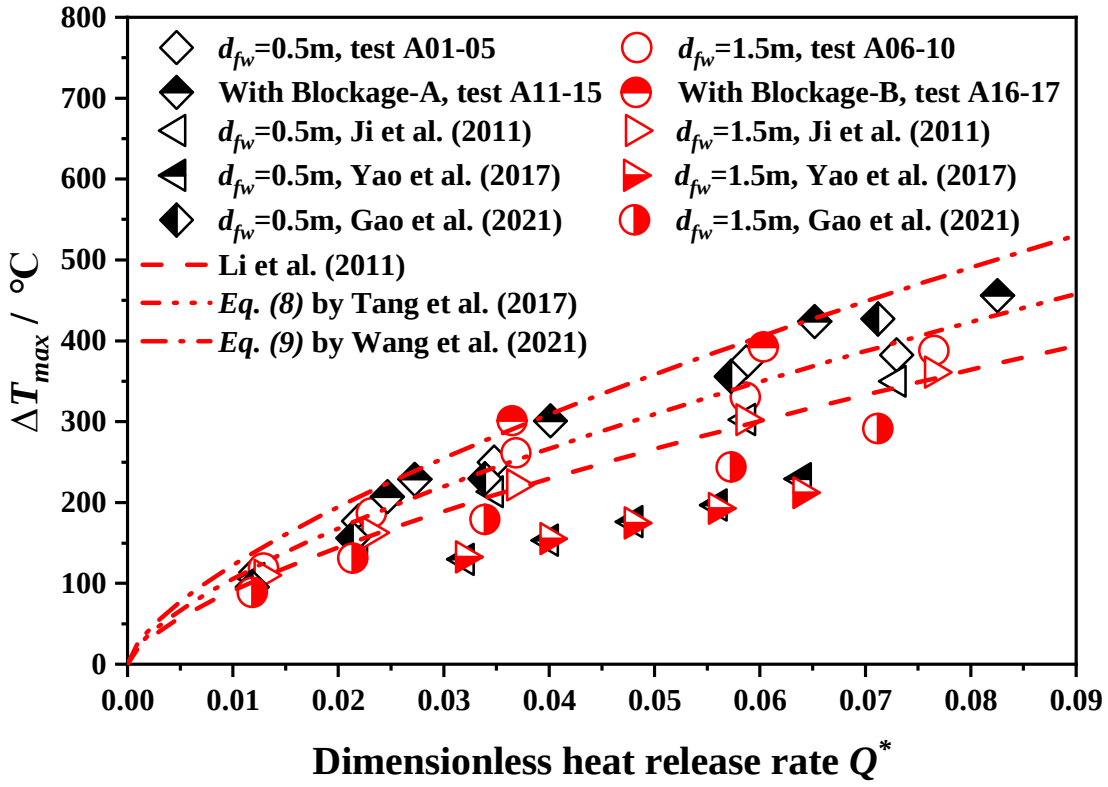

Figure 8. ΔT_{max} in the previous and present work (horizontal tunnels).

Figure 9 further plots the measurements of ceiling temperatures from both the reduced scale tests and simulations carried out in the horizontal tunnels. The plotted data from Figure 9-(a) indicate that ceiling temperatures are generally high when the blockage is placed 0.2 m upstream of the fire. The maximum temperature of the test condition with blockage is about 60 ℃ higher than the values obtained from the pool fires burned without blockage. Meanwhile, ceiling temperatures in the tests considering Blockage A are also slightly higher than the values obtain from tests with Blockage B. This is likely because heat load exhibited in Table 3 denotes that pool fires burned with Blockage A generate a slightly higher value of fuel burning rate, e.g., 0.270 g/s (with Blockage A) versus 0.248 g/s (with Blockage B) for the 12 cm × 12 cm pool fire and 0.439 g/s (with Blockage A) versus 0.406 g/s (with Blockage B) for the 15 cm × 15 cm pool fire. The increase of fuel burning rate is indeed the main reason leading to the increase of ceiling temperatures. However, once the heat release rates are set as constant values, i.e., fires simulated in FDS tests, the plotted values in Figure 9-(b) denote that the maximum temperature of the fire with certain heat release rate are less affected by the blockage effect, implying that burning rate of the pool fire has dominate effect on the maximum temperature while the blockage is the important factor to affect fuel burning rate by

1 influencing the heat feedback.

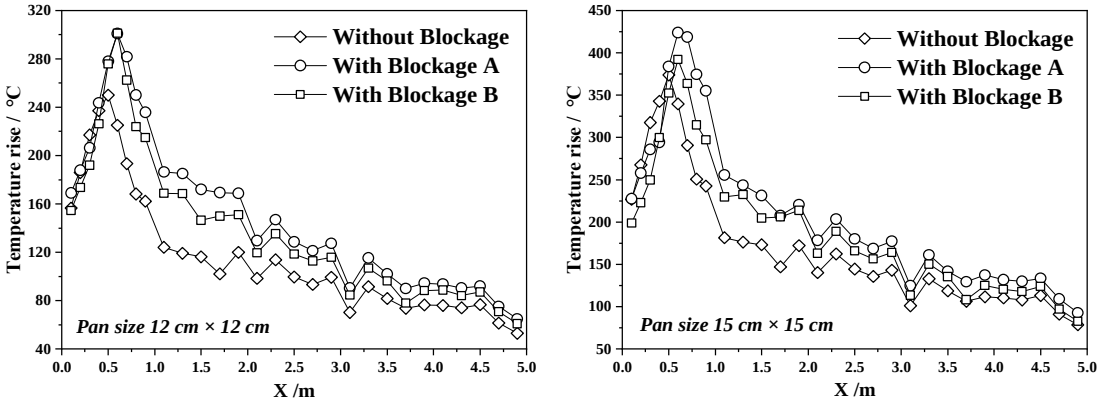

2

3 (a) Experimental results

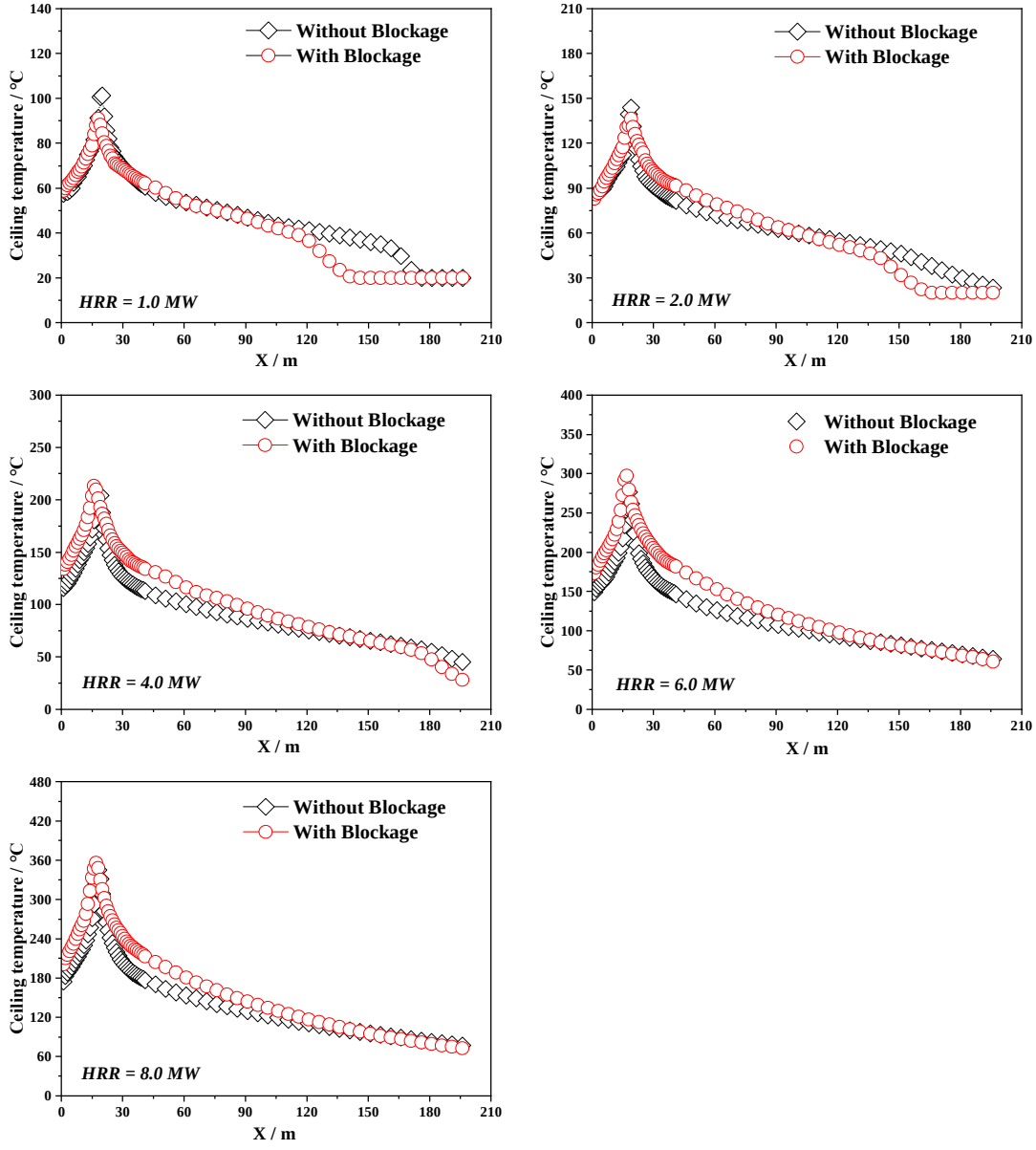

4

(b) FDS simulated results

Figure 9. Ceiling temperatures affected by the blockage effect in horizontal tunnels.

4.2 Effects of tunnel slope

As tunnel slope changes, the interaction between the smoke layer and induced airflow caused by stack effect can lead to different thermal characteristics beneath the ceiling. Figure 10 plots the temperature contours considering the coupling effect of blockage and tunnel slope on the thermal smoke movement. Apparently, the interface of smoke layer within the closed end and blockage descends as tunnel slope increases. When tunnel slope increases to 6%, the fire smoke descend becomes relatively fast and almost touches the ground. Meanwhile, the smoke layer upstream of the fire is also observed to descend to the top of the blockage as tunnels slope increases from 1% to 6%. The reason behind can be explained as the downward movement of smoke being retarded by the buoyancy force along X axis, which finally results in the heat and smoke accumulation. Besides, the total length of the smoke plume impingement increases with the increase of the tunnel slope. It should also be noted that the measurements shown in Figure 6 have already denoted such increase of smoke impingement length caused by the occurrence of blockage. In other words, higher temperature region at tunnel ceiling will largely expand due to the coupling effect of blockage and tunnel slope, underlining that the tunnel under such fire scenario is exposed to higher fire risk.

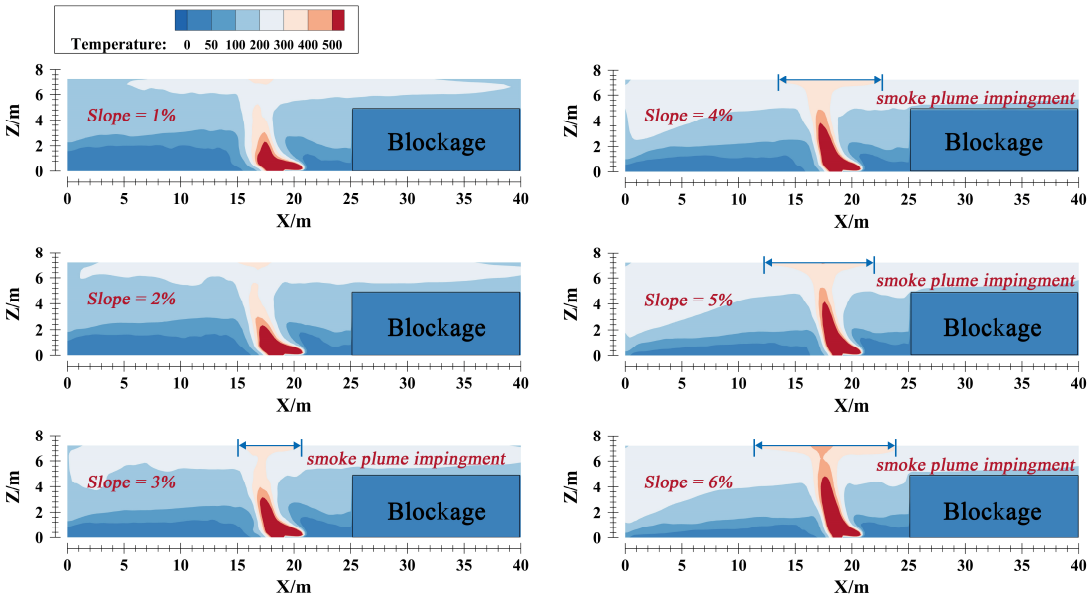

Figure 10. Zoom-in view of temperature contour: effect of slope (HRR = 6.0 MW).

Figure 11 displays ceiling temperatures in both uphill and downhill tunnels under different heat release rates. Firstly, it is very interesting to find out that in Figure 11-(a) the maximum temperature increases as tunnel slope increases in the downhill tunnel while it is less affected by tunnel slope in the uphill tunnel. Such phenomenon looks like contradictory with some previous investigation, e.g., Eq. (5) proposed by Hu et al. (2013) and Eq. (7) established by Wang et al. (2020), where results denote that the maximum temperature is expected to decrease as tunnel slope increases. Such difference might have been caused by several reasons: 1) in the previous studies, fires are burned in tunnels with two openings without any blockage inside. The induced airflow can directly interact with the fire plume and thus achieve very good cooling effect. Correspondingly, the maximum temperature decreases as tunnel slope increases wherever the fire is placed in either uphill or downhill tunnels; 2) when the fire burns between the closed end and blockage in the downhill tunnel, smoke movement upstream of the fire is restrained as the component of buoyancy force parallel to the ceiling is in the opposite direction of smoke spreading towards the tunnel opening. Furthermore, even though the spread of induced airflow is promoted due to the stack effect, blockage upstream of the fire still reduces the cooling effect. As a result, the maximum temperature in downhill tunnels significantly increases attributed to the heat accumulation caused by tunnel slope, blockage, and the closed end. 3) when similar fire scenarios take place in the uphill tunnel, buoyancy force along the X axis becomes the positive force to facilitate the smoke emission through upstream opening. Heat accumulation under such condition is largely relieved. However, cooling effect is still restricted because the spread of induced airflow is impeded by both the stack effect and blockage effect. Correspondingly, values of the maximum temperature in the uphill tunnel shows very limited fluctuation.

Besides, it can also be seen in Figure 11 that ceiling temperatures can be roughly divided into two different regions. In Region I, ceiling temperature increases with tunnel slope. On the contrary, ceiling temperature in Region II decreases as tunnel slope increases. Overall, ceiling temperatures denote a faster temperature decay as tunnel slope increases, implying that the attenuation coefficient κ in Eq. (2) has a strong relationship with tunnel slope. According to the above analysis, it is reasonable to conclude that the coupling effect of blockage and tunnel slope has great influence on both the maximum temperature and ceiling temperature attenuation in the downhill tunnels. To

capture the basic thermal characteristics under such fire scenarios, quantified analysis is then carried out in the following section. To be noted, since the influence of tunnel slope on the maximum temperature is very limited in uphill tunnels, tunnel slope with negative values will thus not be further addressed in the following discussions.

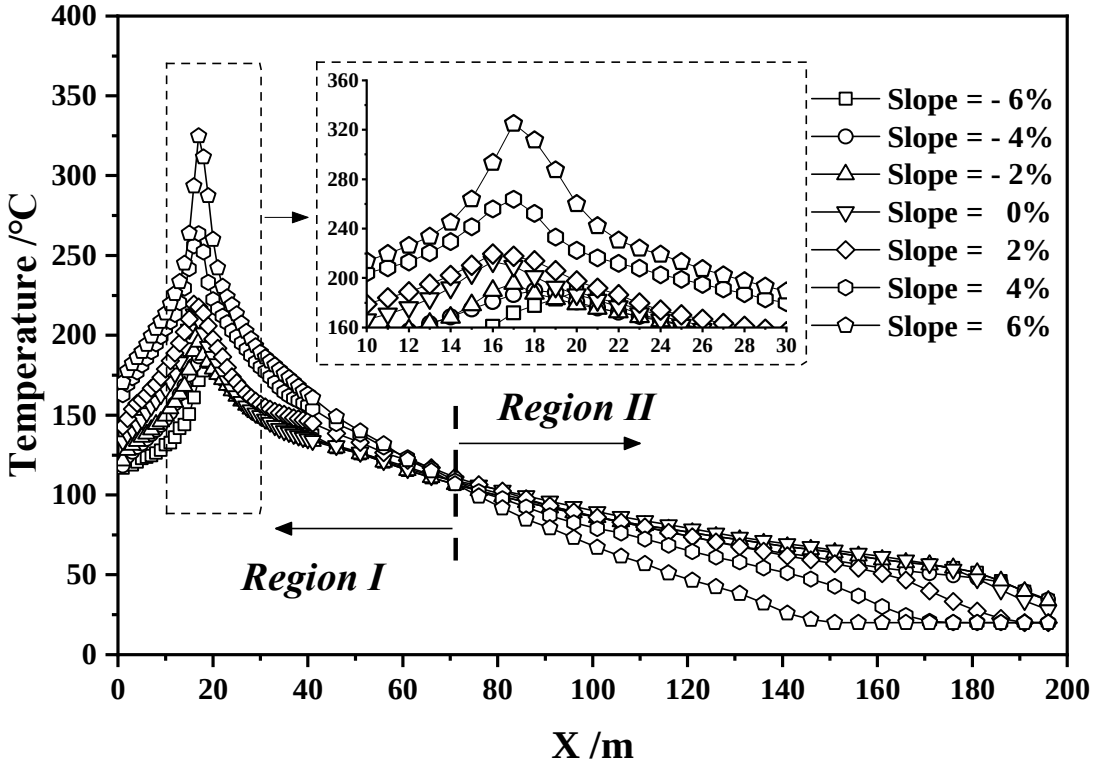

(a) Ceiling temperatures in uphill and downhill tunnels (HRR=4.0 MW)

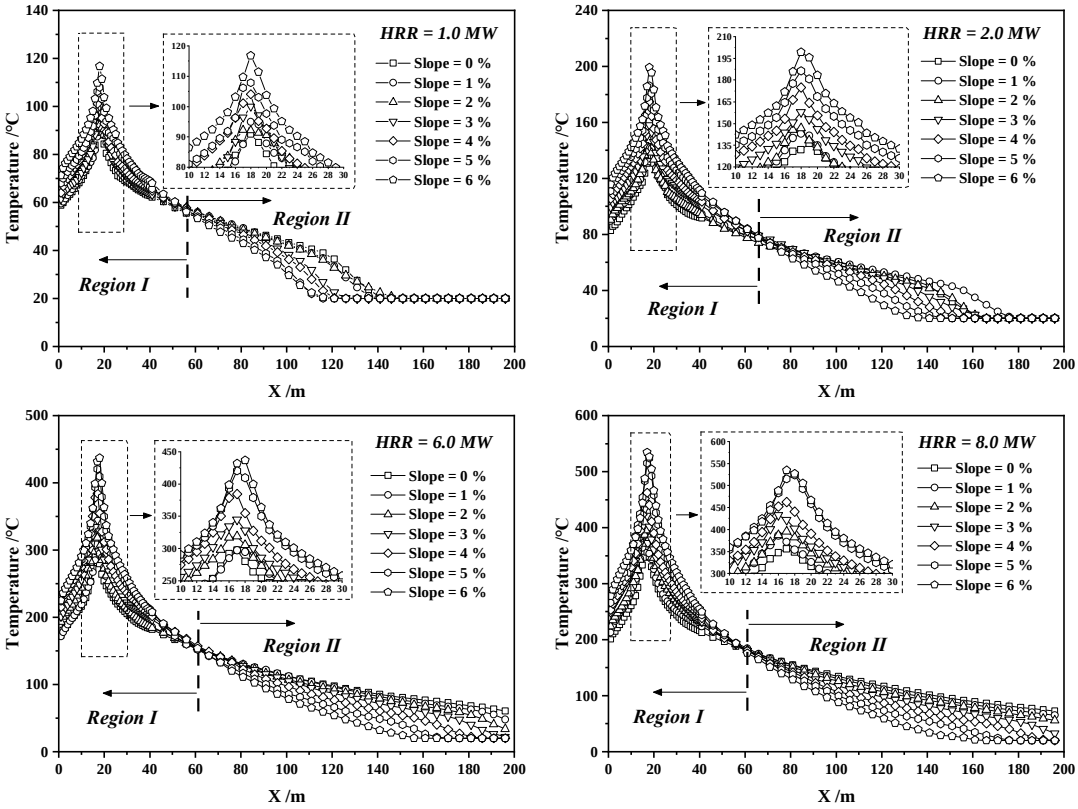

(b) Ceiling temperatures in downhill tunnels

Figure 11. Ceiling temperatures affected by tunnel slope.

As concluded in Figure 8, the maximum temperature of the pool fire burned in a horizontal tunnel with one closed end and blockage, i.e., $\Delta T_{max,b}$, can be very well predicted by Eq. (9) proposed by Wang et al. (2021). When tunnel slope is considered, coefficient ψ is further introduced to quantify the influence of tunnel slope θ. Correspondingly, the maximum temperature considering the closed end, blockage, and tunnel slope, i.e., $\Delta T_{max,sb}$, can be simply expressed as:

$$\Delta T_{max,sb} = \psi \cdot \Delta T_{max,b} \tag{12}$$

with $\psi = f(\theta)$. By plotting the dimensionless temperature ratio of $\Delta T_{max,sb}$ to $\Delta T_{max,b}$ in Figure 12, it can be seen that values of $\frac{\Delta T_{max,sb}}{\Delta T_{max,b}}$ has a strong linear relationship with tunnels slope θ and is less affected by heat release rate, which is consistent with Hu et al. (2013)'s finding shown in Eq. (5). Therefore, $\Delta T_{max,sb}$ can be calculated through a simply linear fitting as

$$\Delta T_{max,sb} = (1.0 + 0.0786\theta) \cdot \Delta T_{max,b} \tag{13}$$

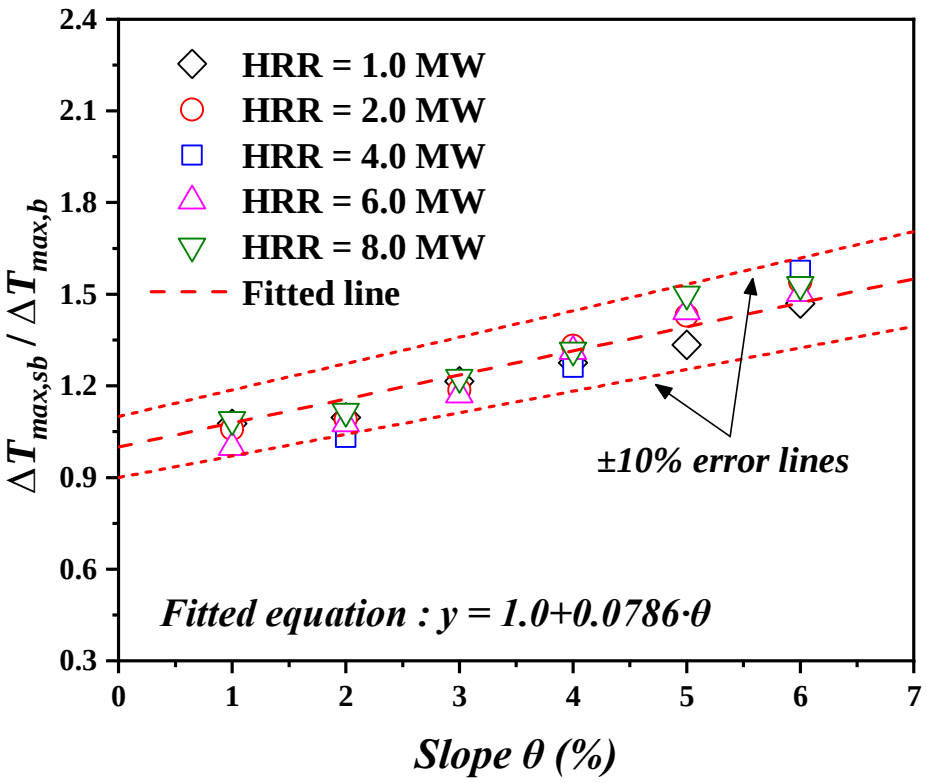

Figure 12. Correlation with tunnel slope for amending maximum gas temperature rise equation based on Eq. (9).

Previous investigation concluded that ceiling temperature attenuation follows the exponential decay. Hu et al. (2005)'s model generated as Eq. (2), in particular, has been widely utilized to predict the ceiling temperatures as it is very simple in expression. In the former discussion, Figure 11 indicates an underlying relationship between the attenuation factor κ in Eq. (2) and tunnel slope θ. Hence, modified attenuation factors λ_θ and k_θ are then introduced to account for the influence caused by tunnel slope. Correspondingly, the dimensionless temperature attenuation upstream of the fire can be expressed as:

$$\frac{\Delta T_x}{\Delta T_{max,sb}} = \lambda_\theta \cdot exp\,(k_\theta \cdot \frac{x}{H_{ef}}) \tag{14}$$

Figure 13 shows the dimensionless temperature attenuation measured in simulations with correlation curves by Eq. (14). The good agreement between measurements and fitted curves indicates that ceiling temperatures under such fire scenario still follow the exponential attenuation and decays faster as tunnel slope increases. Thereafter, values of λ_θ and k_θ obtained from every fitted curve are then summarized in Figure 14. In Figure 14-(a), it can be seen that all the values of λ_θ approximately ranges within 0.83~0.92, i.e., $\pm$5% of the averaged value of λ_θ. Such small fluctuation indicates that λ_θ is insignificantly affected by either tunnel slope or heat release rate.

To simplify the calculation, the averaged value $\overline{\lambda_\theta}$ is directly used. Meanwhile, in Figure 14-(b), values of k_θ under a given tunnel slope are closely gathered regardless of the heat release rate. As tunnel slope increases, values of k_θ perform a sharp decrease which can be well illustrated by a linear fitting calculated as:

$$k_\theta = -0.072 - 0.0162 \cdot \theta \tag{15}$$

Further, by combing the averaged value $\overline{\lambda_\theta}$ and Eq. (15), the dimensionless ceiling temperature attenuation is then generated as:

$$\frac{\Delta T_x}{\Delta T_{max,sb}} = 0.877 \cdot exp\left[-(0.072 + 0.0162 \cdot \theta) \cdot \frac{x}{H_{ef}}\right] \tag{16}$$

Combing Eq. (13) and (16), ceiling temperatures at any location upstream of the fire are then determined.

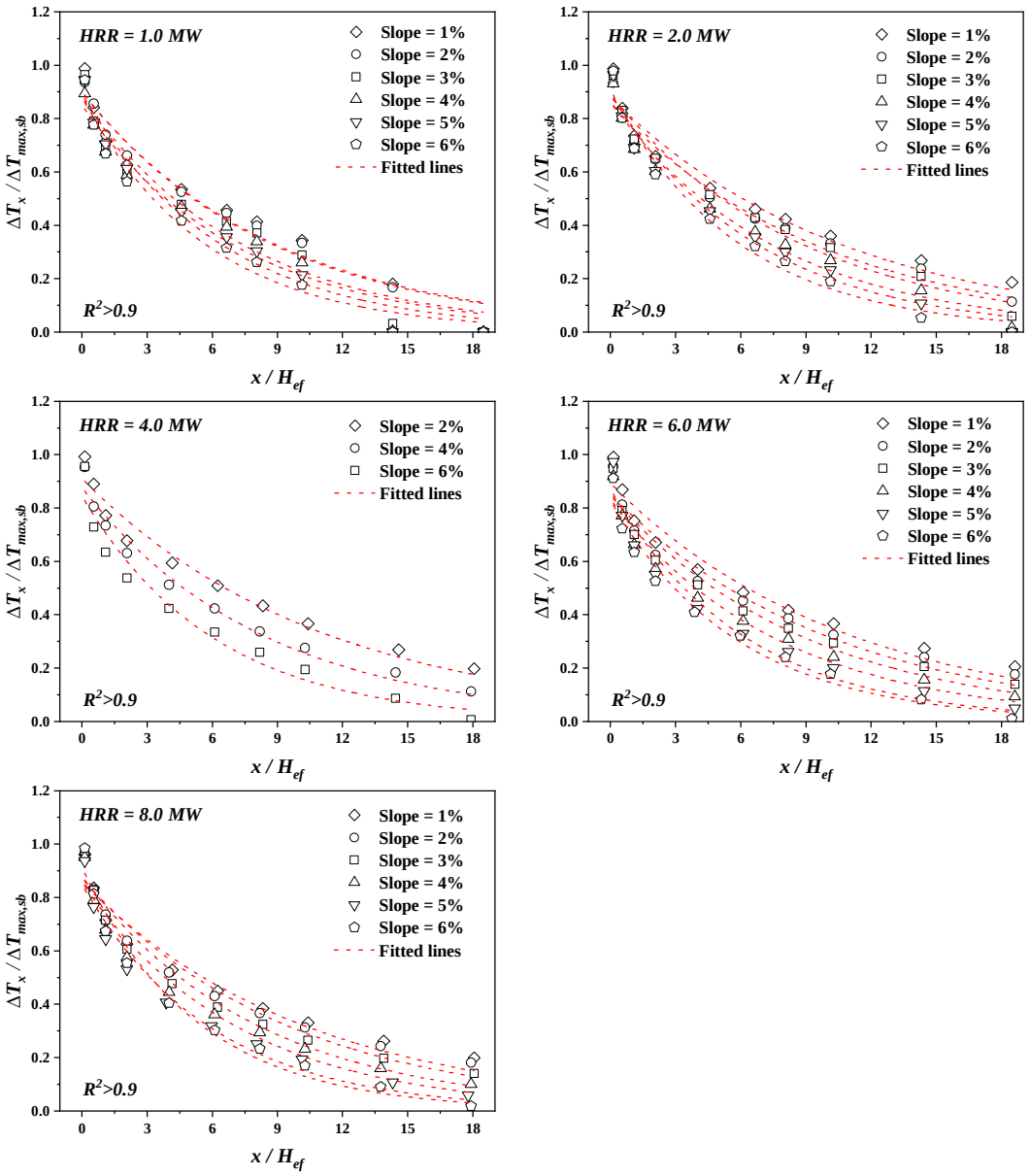

Figure 13. Ceiling temperature attenuation versus tunnel slope θ.

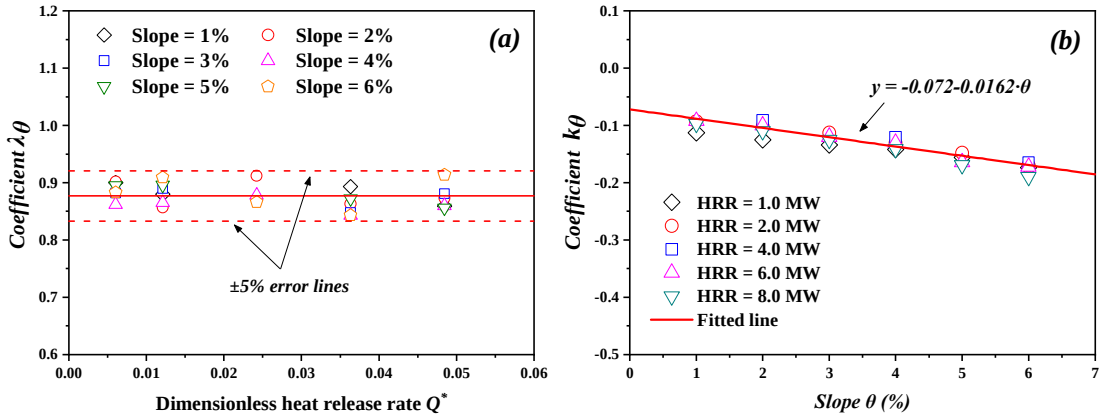

Figure 14. Values of fitting coefficients: (a) coefficient λ_θ; (b) coefficient k_θ.

Figure 15 displays the comparison among the measured and predicted ceiling temperatures in the present work and models established in the previous literature, e.g., Delichatsios (1981), Ingason and Li (2010), Liu et al. (2016), and Wang et al. (2020). As shown in Figure 15-(a), the plotted data mostly distribute within ±10% of the simulated values, denoting convincible predicting results. Meanwhile, the dimensionless temperature attenuation $\frac{\Delta T_x}{\Delta T_{x0}}$ in Figure 15-(b) presents different results and Eq. (16) locates within an acceptable range among the previous models. Such difference of predictions is probably because they were derived with the measurements and physics for different fire scenarios, i.e., corridor fires in Delichatsios (1981), typical tunnel fires in Ingason and Li (2010), fires burned in tunnels with different cross-sections in Liu et al. (2016), and fires burned in a titled tunnel in Wang et al. (2020). To be noted, curves drawn in Figure 15-(b) only represent the condition that tunnel slope θ being 4% for example. Comparisons regarding other tunnel slopes also perform similar results so that they are not exhibited here.

In short, Eq. (13) and (16) established by the correlation of present measurements are dependable to estimate the ceiling temperature profiles for the fire scenario investigated in the present work, i.e., fires burned in a metro depot considering the coupling effect of blockage and tunnel slope. Correspondingly, fire risk in such situation can be evaluated and further ventilation strategies can be made. As an engineering-oriented study, outcomes of the present work are useful in optimizing the design of ventilation system and rescue plan. However, it should be kept in mind that Eq. (13) and (16) were established based on the fire load and tunnel slope respectively distributing within 1.0 MW~8.0 MW and 1%~6%. Special care should be taken when it is used for fire scenarios outside this range.

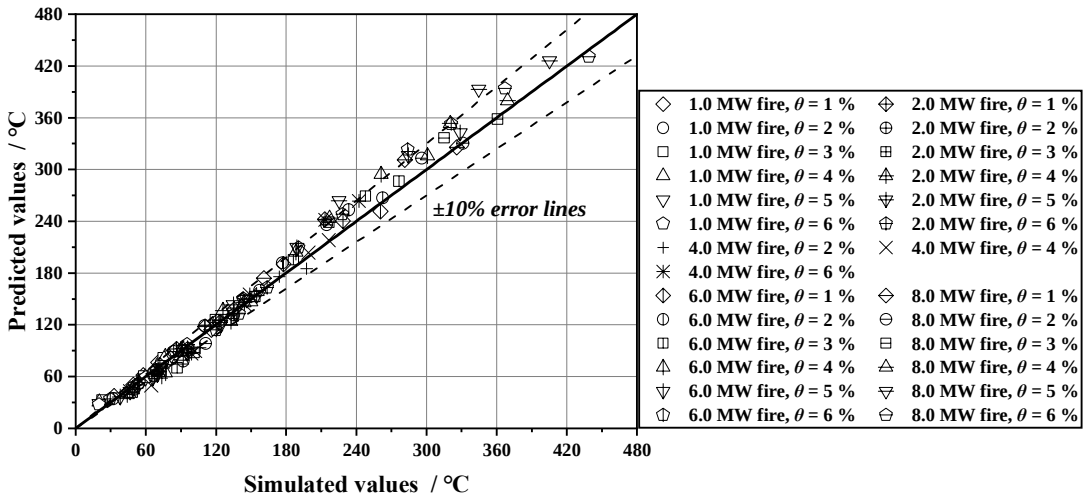

(a) measurements and predicted ceiling temperatures

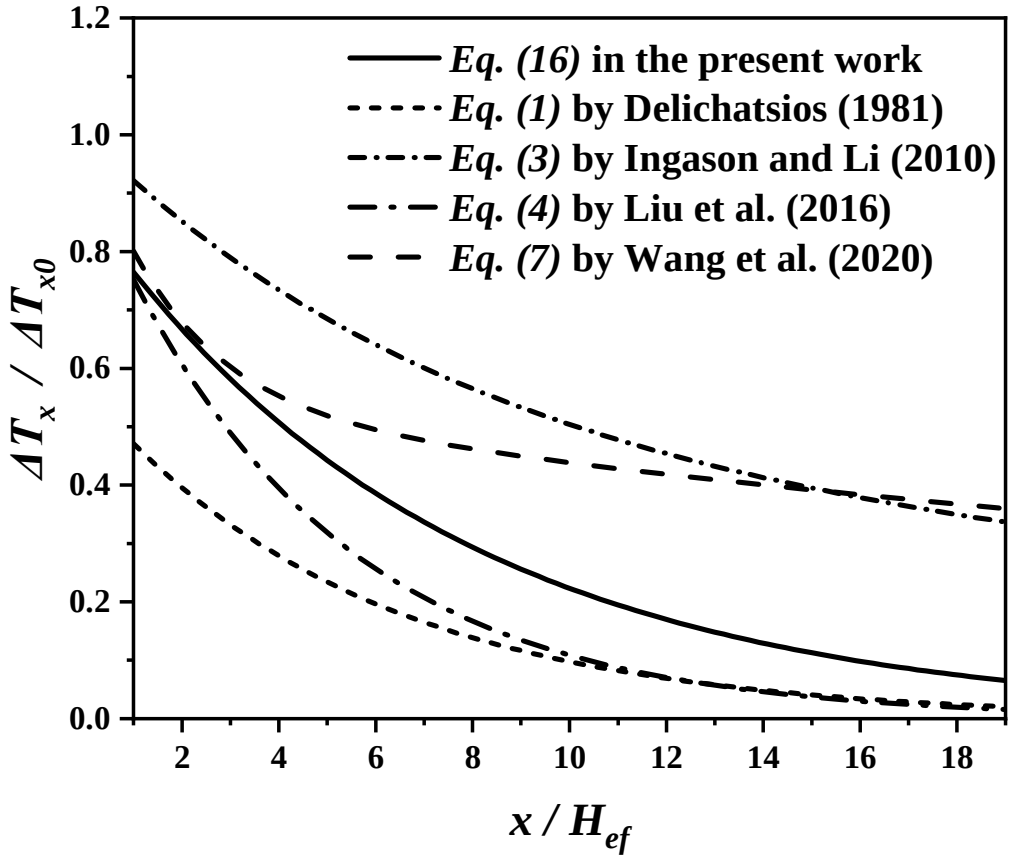

(b) predicted ceiling temperature decay and literature formulas

Figure 15. Comparison among measurements, predicted values and literature formulas.

5. Conclusion

A series of reduced scale burning tests and full-scale CFD simulations were carried out in a metro depot with one closed end. Fuel burning rate and ceiling temperatures were measured and the flame shape was captured to quantify the influence of blockage and tunnel slope on the fire smoke behavior and ceiling temperature distribution. Two empirical correlations were also established to predict the maximum temperature and temperature attenuation beneath the ceiling. Key findings are summarized as follows:

1) The blockage placed upstream of the fire would increase the heat accumulation between the closed end and fire as well as increase flame heat feedback to the pool, leading to the increase of fuel burning rate. Such effect would result in higher ceiling temperatures and affect the smoke movement near the fire source, which results in the unsteady swing of the fire plume and the elevated interface of smoke-air layer.

2) The maximum ceiling temperature increases with the increase of tunnel slope in the downhill tunnel but less affected by the increase of tunnel slope in the uphill tunnel. Meanwhile, in the downhill tunnel, ceiling temperature upstream of the fire decreases faster as tunnel slope increases. Two empirical models are then established to estimate the maximum temperature and ceiling temperature upstream of the fire, accounting for the block effect and tunnel slope.

Declaration of interest

The authors declare that they have no known competing financial interests or personal relationships that could have appeared to influence the work reported in this paper.

Acknowledgement

This work was supported by Graduate Scientific Research and Innovation Foundation of Chongqing, China (Grant No. CYB20029, CYS19009), Chongqing Science and Technology Commission (Grant No. cstc2019jscx-msxmX0243) and Chongqing Construction Science and Technology Planning Project 459 (Grant No. 2019(1-5-5)).

Jiaqiang Han also acknowledges the financial support of China Scholarship Council under the Program for Ph.D. Student Overseas Study Scholarship 2020 (Grant No. 202006050098), which facilitate his study at Warwick Fire, School of Engineering at University of Warwick.

Appendix A. Uncertainty analysis

The uncertainty analysis was carried out on the basis of the root-sum-square (RSS) method proposed by Kline and Mcclintock (1953). When the result R of experiment is assumed to be a function of a set of measuring variables, which can be expressed as

$$R = f(x_1, x_2, \dots x_{n-1}, x_n,) \quad \text{(A-1)}$$

Then the overall uncertainty in the result δR can be determined by the combination of uncertainty contributed from each variable, which is generated as

$$\delta R = \left(\sum_{i=1}^{n} \left(\frac{\partial R}{\partial x_i}\delta x_i\right)^2\right)^{1/2} \quad \text{(A-2)}$$

Where δx_i is the absolute uncertainty of the measured variable x_i.

If R can be calculated in a pure product form of the measured values (Moffat, 1988)

$$R = {x_1}^a {x_2}^b {x_3}^c \dots {x_M}^m \quad \text{(A-3)}$$

Then

$$\frac{\delta R}{R}=\left\{\left\{\left(a\frac{\delta x_1}{x_1}\right)^2+\left(b\frac{\delta x_2}{x_2}\right)^2+\cdots+\left(m\frac{\delta x_m}{x_m}\right)^2\right\}\right\}^{1/2} \tag{A-4}$$

Thereafter, the uncertainty of measurements in the study at hand could be estimate as follows.

(1) Uncertainty of the burning rate measurement

According to the study of Shafee and Yozgatligil (2018b), the fuel burning rate per unit area of a pool fire can be calculated as

$$\dot{m}''=\frac{\Delta m}{\Delta t\cdot A} \tag{A-5}$$

where Δm is the mass loss, Δt is the time interval, and A is the area of burning surface.

Then the uncertainty of the burning rate measurement can be calculated based on Eq. (A-2) as

$$\delta\dot{m}''=\pm\left[\left(\frac{\partial\dot{m}''}{\partial\Delta m}\delta\Delta m\right)^2+\left(\frac{\partial\dot{m}''}{\partial\Delta t}\delta\Delta t\right)^2+\left(\frac{\partial\dot{m}''}{\partial\Delta A}\delta\Delta A\right)^2\right]^{1/2} \tag{A-6}$$

where $\frac{\partial\dot{m}''}{\partial\Delta m}=\frac{1}{\Delta t\cdot A}$, $\frac{\partial\dot{m}''}{\partial\Delta t}=\frac{-\Delta m}{(\Delta t)^2\cdot A}$, $\frac{\partial\dot{m}''}{\partial A}=\frac{-\Delta m}{\Delta t\cdot A^2}$.

Based on Eq. (A-6), the relative uncertainty of measured burning rate, namely $\frac{\delta\dot{m}''}{\dot{m}''}$, can be therefore obtained as

$$\frac{\delta\dot{m}''}{\dot{m}''}=\pm\left[\left(\frac{\partial\dot{m}''}{\partial\Delta m}\frac{\delta\Delta m}{\Delta m}\frac{\Delta m}{\dot{m}''}\right)^2+\left(\frac{\partial\dot{m}''}{\partial\Delta t}\frac{\delta\Delta t}{\Delta t}\frac{\Delta t}{\dot{m}''}\right)^2+\left(\frac{\partial\dot{m}''}{\partial A}\frac{\delta A}{A}\frac{A}{\dot{m}''}\right)^2\right]^{1/2} \tag{A-7}$$

where $\frac{\delta\Delta m}{\Delta m}$, $\frac{\delta\Delta t}{\Delta t}$, and $\frac{\delta A}{A}$ are respectively the relative uncertainties of the measured mass loss, time interval in the steady stage, and pool surface area.

The relative uncertainty of measured fuel mass was mainly determined by balance readability, linearity, and repeatability. All the values are $\pm$ 0.1g referred to the technical guide of electronic balance. Further, the uncertainties of measured time interval and fuel pans area are determined by the load cell resolution of $\pm$ 0.2s and the ruler resolution of $\pm$ 1 mm. By taking these values in to generation of Eq. (A-7), the maximum relatively uncertainty of the burning rate is less than $\pm$5 %

(2) Uncertainty of the temperature measurement

In the current study, temperature values were measured by K-type thermocouples whose uncertainty of temperature reading was $\pm$ 0.1 ℃. Meanwhile, a conservative value of $\pm$ 1 ℃ was considered herein and the relative uncertainty of temperature is calculated as $\frac{\delta T}{T}=\pm(\frac{\pm 1\ ℃}{T\ (℃)})$. Since

all the burning tests were conducted under a very similar environmental condition with ambient temperature around 20 ℃, the maximal relatively uncertainty of temperature measurement is about ± 5.0 %.

Reference

An, W., Li, S., Yin, X., Peng, L., 2021. Combustion and fire safety of energy conservation materials in building vertical channel: Effects of structure factor and coverage rate. Case Studies in Thermal Engineering 24.

Atkinson, G.T., Wu, Y., 1996. Smoke control in sloping tunnels. Fire Safety Journal 27, 335-341.

Barbato, L., Cascetta, F., Musto, M., Rotondo, G., 2014. Fire safety investigation for road tunnel ventilation systems – An overview. Tunnelling and Underground Space Technology 43, 253-265.

Cheng, X., Shi, Z., Nguyen, K., Zhang, L., Zhou, Y., Zhang, G., Wang, J., Shi, L., 2020. Solar chimney in tunnel considering energy-saving and fire safety. Energy 210.

Delichatsios, M.A., 1981. The flow of fire gases under a beamed ceiling. Combustion and Flame 43, 1-10.

Fan, C.G., Ji, J., Sun, J.H., 2015. Influence of longitudinal fire location on smoke characteristics under the tunnel ceiling. Fire and Materials 39, 72-84.

Gannouni, S., Maad, R.B., 2015. Numerical study of the effect of blockage on critical velocity and backlayering length in longitudinally ventilated tunnel fires. Tunnelling and Underground Space Technology 48, 147-155.

Gannouni, S., Zinoubi, J., Ben Maad, R., 2019. Numerical study on the thermal buoyant flow stratification in tunnel fires with longitudinal imposed airflow: Effect of an upstream blockage. International Journal of Thermal Sciences 136, 230-242.

Gao, Z., Li, L., Zhong, W., Liu, X., 2021. Characterization and prediction of ceiling temperature propagation of thermal plume in confined environment of common services tunnel. Tunnelling and Underground Space Technology.

Gao, Z.H., Ji, J., Fan, C.G., Sun, J.H., Zhu, J.P., 2014. Influence of sidewall restriction on the maximum ceiling gas temperature of buoyancy-driven thermal flow. Energy and Buildings 84, 13-20.

Han, J., Geng, P., Wang, Z., Wang, F., Weng, M., Liu, F., 2021. Effects of fire-blockage distance on pool fire burning behavior and thermal temperature profiles in a naturally ventilated tunnel. Tunnelling and

Underground Space Technology 117.

Han, J., Liu, F., Wang, F., Weng, M., Wang, J., 2020. Study on the smoke movement and downstream temperature distribution in a sloping tunnel with one closed portal. International Journal of Thermal Sciences 149.

Hu, L.H., Chen, L.F., Wu, L., Li, Y.F., Zhang, J.Y., Meng, N., 2013. An experimental investigation and correlation on buoyant gas temperature below ceiling in a slopping tunnel fire. Applied Thermal Engineering 51, 246-254.

Hu, L.H., Huo, R., Li, Y.Z., Wang, H.B., Chow, W.K., 2005. Full-scale burning tests on studying smoke temperature and velocity along a corridor. Tunnelling and Underground Space Technology 20, 223-229.

Huang, Y., Li, Y., Dong, B., Li, J., Liang, Q., 2018. Numerical investigation on the maximum ceiling temperature and longitudinal decay in a sealing tunnel fire. Tunnelling and Underground Space Technology 72, 120-130.

Ingason, H., Li, Y.Z., 2010. Model scale tunnel fire tests with longitudinal ventilation. Fire Safety Journal 45, 371-384.

Ingason, H., Li, Y.Z., 2019. Large scale tunnel fire tests with different types of large droplet fixed fire fighting systems. Fire Safety Journal 107, 29-43.

Ingason, H., Li, Y.Z., Lnnermark, A., 2015. Tunnel Fire Dynamics. Springer New York.

Ishikawa, T., Kasumi, K., Tanaka, F., 2020. Effects of Tunnel Length on Combustion Efficiency in Tunnel Fires. Springer Singapore, Singapore, pp. 1075-1088.

Ji, J., Fan, C.G., Zhong, W., Shen, X.B., Sun, J.H., 2012. Experimental investigation on influence of different transverse fire locations on maximum smoke temperature under the tunnel ceiling. International Journal of Heat and Mass Transfer 55, 4817-4826.

Ji, J., Zhong, W., Li, K.Y., Shen, X.B., Zhang, Y., Huo, R., 2011. A simplified calculation method on maximum smoke temperature under the ceiling in subway station fires. Tunnelling and Underground Space Technology 26, 490-496.

Kline, S.J., Mcclintock, F.A., 1953. Describing Uncertainties in Single-Sample Experiments. Mechanical engineering (New York, N.Y.: 1919) 75.

Kurioka, H., Oka, Y., Satoh, H., Sugawa, O., 2003. Fire properties in near field of square fire source with longitudinal ventilation in tunnels. Fire Safety Journal 38, 319-340.

Li, Y.Z., Lei, B., Ingason, H., 2010. Study of critical velocity and backlayering length in longitudinally

ventilated tunnel fires. Fire Safety Journal 45, 361-370.

Li, Y.Z., Lei, B., Ingason, H., 2011. The maximum temperature of buoyancy-driven smoke flow beneath the ceiling in tunnel fires. Fire Safety Journal 46, 204-210.

Liu, C., Zhong, M., Song, S., Xia, F., Tian, X., Yang, Y., Long, Z., 2020. Experimental and numerical study on critical ventilation velocity for confining fire smoke in metro connected tunnel. Tunnelling and Underground Space Technology 97.

Liu, C., Zhong, M., Tian, X., Zhang, P., Xiao, Y., Mei, Q., 2019. Experimental and numerical study on fire-induced smoke temperature in connected area of metro tunnel under natural ventilation. International Journal of Thermal Sciences 138, 84-97.

Liu, F., Yu, L.X., Weng, M.C., Lu, X.L., 2016. Study on longitudinal temperature distribution of fire-induced ceiling flow in tunnels with different sectional coefficients. Tunnelling and Underground Space Technology 54, 49-60.

Long, Z., Yang, Y., Liu, C., Zhong, M., 2020. Study on the optimal operation mode of ventilation system during metro double-island platform fire. Building Simulation.

McGrattan, K., McDermott, R., Hostikka, S., Floyd, J., Vanella, M., Weinschenk, C., Overholt, K., 2018. Fire Dynamics Simulator User's Guide. NIST special publication 1019.

McGrattan, K.B., Baum, H.R., Rehm, R.G., 1998. Large eddy simulations of smoke movement. Fire Safety Journal 30, 161-178.

Mehaddi, R., Collin, A., Boulet, P., Acem, Z., Telassamou, J., Becker, S., Demeurie, F., Morel, J.Y., 2020. Use of a water mist for smoke confinement and radiation shielding in case of fire during tunnel construction. International Journal of Thermal Sciences 148.

Moffat, R.J., 1988. Describing the uncertainties in experimental results. Experimental Thermal and Fluid Science 1, 3-17.

Nævestad, T.-O., Meyer, S., 2014. A survey of vehicle fires in Norwegian road tunnels 2008–2011. Tunnelling and Underground Space Technology 41, 104-112.

Oka, Y., Atkinson, G.T., 1995. Control of smoke flow in tunnel fires. Fire Safety Journal 25, 305-322.

Rojas Alva, W.U., Jomaas, G., Dederichs, A.S., 2017. The influence of vehicular obstacles on longitudinal ventilation control in tunnel fires. Fire Safety Journal 87, 25-36.

Saito, S., Yamauchi, Y., 2021. Numerical study of the influence of tunnel wall properties on ceiling jet temperature in tunnel fires. Tunnelling and Underground Space Technology 116.

Seike, M., Kawabata, N., Hasegawa, M., Tanaka, H., 2019. Heat release rate and thermal fume behavior estimation of fuel cell vehicles in tunnel fires. International Journal of Hydrogen Energy 44, 26597-26608.

Shafee, S., Yozgatligil, A., 2018a. An analysis of tunnel fire characteristics under the effects of vehicular blockage and tunnel inclination. Tunnelling and Underground Space Technology 79, 274-285.

Shafee, S., Yozgatligil, A., 2018b. An experimental study on the burning rates of interacting fires in tunnels. Fire Safety Journal 96, 115-123.

Shi, C., Zhong, M., Chen, C., Jiao, W., Li, J., Zhang, Y., Zhang, L., Li, Y., He, L., 2020. Metro train carriage combustion behaviors – Full-scale experiment study. Tunnelling and Underground Space Technology 104.

Tanaka, F., Majima, S., Kato, M., Kawabata, N., 2015. Performance validation of a hybrid ventilation strategy comprising longitudinal and point ventilation by a fire experiment using a model-scale tunnel. Fire Safety Journal 71, 287-298.

Tang, F., Cao, Z.L., Chen, Q., Meng, N., Wang, Q., Fan, C.G., 2017. Effect of blockage-heat source distance on maximum temperature of buoyancy-induced smoke flow beneath ceiling in a longitudinal ventilated tunnel. International Journal of Heat and Mass Transfer 109, 683-688.

Tang, F., Hu, P., Wen, J., 2020. Experimental investigation on lateral ceiling temperature distribution induced by wall-attached fire with various burner aspect ratios in underground space. Fire Safety Journal.

Waman, W., Harish, R., 2020. Influence of volume blockage ratio on turbulent buoyant plume dispersion in mixed ventilated tunnel. Journal of Wind Engineering and Industrial Aerodynamics 207.

Wang, J., Wu, Z., Xiao, X., He, Y., 2006. Selection of computational domain in numerical simulation of building fires. Fire Safety Science 15, 232-240.

Wang, Z., Ding, L., Wan, H., Ji, J., Gao, Z., Yu, L., 2020. Numerical investigation on the effect of tunnel width and slope on ceiling gas temperature in inclined tunnels. International Journal of Thermal Sciences 152, 106272.

Wang, Z., Han, J., Wang, J., Geng, P., Weng, M., Liu, F., 2021. Temperature distribution in a blocked tunnel with one closed portal under natural ventilation. Tunnelling and Underground Space Technology 109.

Yao, Y., Cheng, X., Zhang, S., Zhu, K., Zhang, H., Shi, L., 2017. Maximum smoke temperature beneath the ceiling in an enclosed channel with different fire locations. Applied Thermal Engineering 111, 30-38.

Yu, L., Wan, H., Ji, J., 2020. Asymmetric flow effect in a horizontal natural ventilated tunnel with different aspect ratios under the influence of longitudinal fire locations. Building Simulation.

Zhang, S., Shi, L., Li, X., Huang, Y., He, K., Wang, J., 2020. Critical ventilation velocity under the blockage of different metro train in a long metro tunnel. Fire and Materials.

Zukoski, E.E., Kubota, T., Cetegen, B., 1981. Entrainment in fire plumes. Fire safety journal 3, 107-121.